

# Self-similarity of negative particle production from the Beam Energy Scan Program at STAR

M.V. Tokarev

(on behalf of STAR Collaboration)

*Joint Institute for Nuclear Research, Dubna, Russia*

*E-mail: tokarev@jinr.ru*

## Abstract

We present the spectra of negative charged particle production in Au+Au collisions from STAR for the first phase of the RHIC Beam Energy Scan Program measured over a wide range of collision energy  $\sqrt{s_{NN}}=7.7-200$  GeV, and transverse momentum of produced particle in different centralities at  $|\eta| < 0.5$ . The spectra demonstrate strong dependence on collision energy which enhances with  $p_T$ . An indication of self-similarity of negative charged particle production in Au+Au collisions is found. The constituent energy loss as a function of energy and centrality of collisions and transverse momentum of inclusive particle was estimated in the  $z$ -scaling approach. The energy dependence of the model parameters - the fractal and fragmentation dimensions and "specific heat was studied.

PACS: 25.75.-q

Keywords: High energy; heavy ions; hadron spectra; self-similarity; energy loss.

Presented at the International Conference "HADRON STRUCTURE'15" ,  
29 June — 3 July, 2015, Horný Smokovec, Slovak Republic.

## I. INTRODUCTION

A major goal of high-energy heavy-ion collision experiments at RHIC is to determine the phase diagram for nuclear matter and describe its features in framework of the Quantum Chromodynamics (QCD). The most experimentally accessible way to characterize the QCD phase diagram is in the plane of temperature ( $T$ ) and the baryon chemical potential ( $\mu_B$ ) [1].

Heavy-ion collisions at RHIC have provided evidence that a new state of nuclear matter exists at the top RHIC energy  $\sqrt{s_{NN}} = 200$  GeV [2–5]. This new state is characterized by a suppression of particle production at high  $p_T$  [6–9], a large amount of elliptic flow ( $v_2$ ), number-of-constituent-quark (NCQ) scaling of  $v_2$  at intermediate  $p_T$  [10] and enhanced correlated yields at large  $\Delta\eta$  and  $\Delta\phi \simeq 0$  (ridge) [11–13].

Figure 1 shows a schematic layout of the phases, along with hypothesized indications of the regions crossed in the early stages of nuclear collisions at various beam energies.

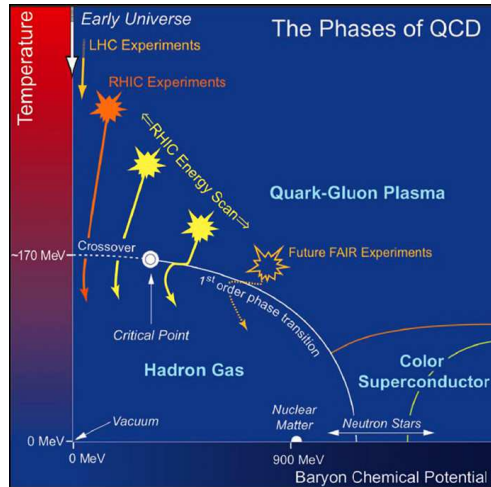


FIG. 1: Phase diagram of nuclear matter [20].

The idea of the Beam Energy Scan (BES) Program at RHIC [14] was to vary the collision energy with aim to search for the QCD critical point and QCD phase boundary [15–19]. The first phase of the Beam Energy Scan program (BES-I) along with the existing top energy at RHIC has allowed the access to a region of the QCD phase diagram (Fig. 1) covering a range of baryon chemical potential ( $\mu_B$ ) from 20 to 420 MeV corresponding to Au+Au collision energies from  $\sqrt{s_{NN}} = 200$  to 7.7 GeV, respectively. Results from BES-I have further supported the evidence for the quark-gluon plasma (QGP) discovery at the top RHIC energy  $\sqrt{s_{NN}} = 200$  GeV [14, 20]. The results of the search for the critical point and the first-order phase boundary have narrowed the region of interest to collision energies below  $\sqrt{s_{NN}} = 20$  GeV.

The principal challenge remains localization of a critical point on the QCD phase diagram. Near the QCD critical point, several thermodynamic properties of the system

such as the heat capacity, compressibility, correlation length are expected to diverge with a power-law behavior in the variable  $\epsilon = (T - T_c)/T_c$ , where  $T_c$  is the critical temperature. The rate of the divergence can be described by a set of critical exponents. The critical exponents are universal in the sense that they depend only on degrees of freedom in the theory and their symmetry, but not on other details of the interactions. This scaling postulate is the central concept of the theory of critical phenomena [21, 22]. Current lattice QCD calculations suggest that key features of the phase diagram like the critical point and the first-order phase transition lie within the  $\mu_B$  reach of the RHIC BES Phase-II program (see [20] and references therein).

## II. EXPERIMENT AND DATA ANALYSIS

The preliminary results presented here are based on data taken at STAR in Au+Au collisions at  $\sqrt{s_{NN}} = 7.7, 11.5, 39, 62.4$  and 200 GeV in the year 2010 while 19.6 and 27 GeV were collected in the year 2011. The transverse momentum spectra of negatively charged particle production in the mid-rapidity over a wide range of centrality are reported in this paper.

### A. STAR detector

The main detector used to obtain the results on particle spectra is the Time Projection Chamber (TPC) [23]. The TPC is the primary tracking device at STAR and can track up to 4000 charged particles per event. It is 4.2 m long and 4 m in diameter. Its acceptance covers  $\pm 1$  units of pseudo-rapidity  $\eta$  and the full azimuthal angle. The sensitive volume of the TPC contains P10 gas (10% methane, 90% argon) regulated at 2 mbar above atmospheric pressure. The TPC data are used to determine particle trajectories, momenta, and particle-type through ionization energy loss ( $dE/dx$ ). STAR's solenoidal magnetic field used for this low energy Au+Au test run was 0.5T. The Time of Flight (ToF) detector [24] (with  $2\pi$  azimuthal coverage and  $|\eta| < 1.0$ ) further enhances the PID capability. All events were taken with a minimum bias trigger. The trigger detectors used in these data are the Beam-Beam-Counter (BBC) and Vertex Position Detector (VPD)[25]. The BBCs are scintillator annuli mounted around the beam pipe beyond the east and west pole-tips of the STAR magnet at about 375 cm from the center of the nominal interaction region (IR), and they have an  $\eta$  coverage of  $3.8 < |\eta| < 5.2$  and a full azimuthal ( $2\pi$ ) coverage. The VPDs are based on the conventional technology of plastic scintillator read-out by photomultiplier tubes. They consist of two identical detector setups very close to the beam pipe, one on each side at a distance of  $|V_z| = 5.6$  m from the center of the IR. The details about the design and the other characteristics of the STAR detector can be found in [23].

All events selected for the analysis satisfied the cuts described below. The primary

Table 1. Track selection criteria at all energies.

$ \eta $	DCA	nFitPts	nFitPts/nFitPoss	ndE/dx	pTpr/pTgl
$< 0.5$	$< 1$ cm	$> 15$	$> 0.52$	$> 10$	$7/10 < \& < 10/7$

vertex for each minimum bias event is determined by finding the best point of common origin of the tracks measured in the TPC. In order to reject events which involve interactions with the beam pipe and beam-gas interactions, the vertex positions along the  $x, y$  and longitudinal ( $z$ ) beam directions are required to be less than 2 cm and 30 cm, respectively.

Track selection criteria for all data sets are presented in Table II A. Primary tracks are placed on the distance of closest approach (DCA) between each track and the event vertex. Tracks must have at least 15 points (nFitPts) used in track fitting. To prevent multiple counting of split tracks, at least 52% of the total possible fit point are required (nFitPts/nFitPoss). A condition is placed on the number of dE/dx points used to derive dE/dx values (ndE/dx). The cut for the  $p_T$  ratio of primary and global tracks (pTpr/pTgl) were used to delete fail tracks. The results presented here are for transverse momentum  $p_T > 0.2$  GeV/ $c$  and pseudo-rapidity  $|\eta| < 0.5$  were selected for the analysis.

The efficiency is determined by measuring the reconstruction efficiency of Monte Carlo tracks embedded in real events and then run through the STAR reconstruction chain including realistic STAR geometry. For a given collision energy, centrality region, and particle species the efficiency is fitted as a function of  $p_T$  using the functional form  $\text{eff} = A \cdot \exp\{-(B/p_T)^C\}$ . The parameters  $A$ ,  $B$ , and  $C$  are determined for each centrality for unidentified particles using efficiencies for identified particles.

Figure 2 demonstrates dependence of reconstruction efficiency on transverse momentum of particle at energy  $\sqrt{s_{NN}} = 7.7$  and 200 GeV and various centralities.

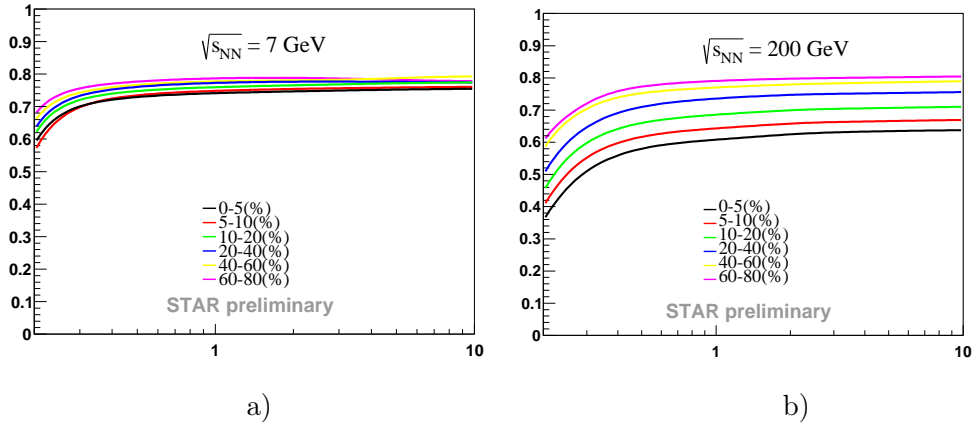


Рис. 2: Reconstruction efficiency of negatively charged particles produced in Au+Au collisions at energies  $\sqrt{s_{NN}} = 7.7$  and 200 GeV in the range  $|\eta| < 0.5$  and various centralities as a function of  $p_T$ .

Centrality classes in Au+Au collisions at  $\sqrt{s_{NN}} = 7.7 - 200$  GeV are defined using the number of charged particle tracks reconstructed in the main TPC over the full azimuth and pseudorapidity  $|\eta| < 0.5$ . This is generally called "reference multiplicity (refmult)" in STAR [26, 27]. For each energy, a refmult "correction" is applied on the standard definition. This is based on the following steps: identifying bad runs, applying acceptance/efficiency correction of refmult for different  $z$ -vertex positions, and performing low refmult correction for trigger inefficiencies for different  $z$ -vertices. The refmult distribution is compared/fitted to Monte-Carlo Glauber model simulations. The centrality is defined by calculating the fraction of the total cross-section obtained from the simulated multiplicity. The events are divided into following centrality classes: 0 – 5%, 5 – 10%, 10 – 20%, 20 – 40%, 40 – 60%, 60 – 80%. Table II A shows the total number of events that are used for the analysis for each energy after the above event selection cuts.

Table 2. Total events analyzed after all analysis cuts for various energies.

$\sqrt{s_{NN}}$ (GeV)	Year	Events (Millions)
7.7	2010	2
11.5	2010	7
19.6	2011	17
27	2011	33
39	2010	108
62.4	2010	62
200	2010	35

### III. RESULTS AND DISCUSSION

#### A. Transverse momentum spectra

The transverse momentum spectrum of hadrons produced in high-energy collisions of heavy ions reflects features of constituent interactions in the nuclear medium. The medium modification is one of the effects (recombination, coalescence, energy loss, multiple scattering,...) that affects the shape of the spectrum. The properties of the created medium are experimentally studied by variation of the event centrality and collision energy.

Figures 3 and 4 shows the negatively charged hadron yields in Au+Au collisions at  $\sqrt{s_{NN}} = 7.7, 11.5, 19.6, 27, 62.4$  and 200 GeV at mid-rapidity  $|\eta| < 0.5$  as a function of transverse momentum  $p_T$ . The results are shown for the collision centrality classes of 0 – 5%, 5 – 10%, 10 – 20%, 20 – 40%, 40 – 60%, 60 – 80%. The distributions are measured

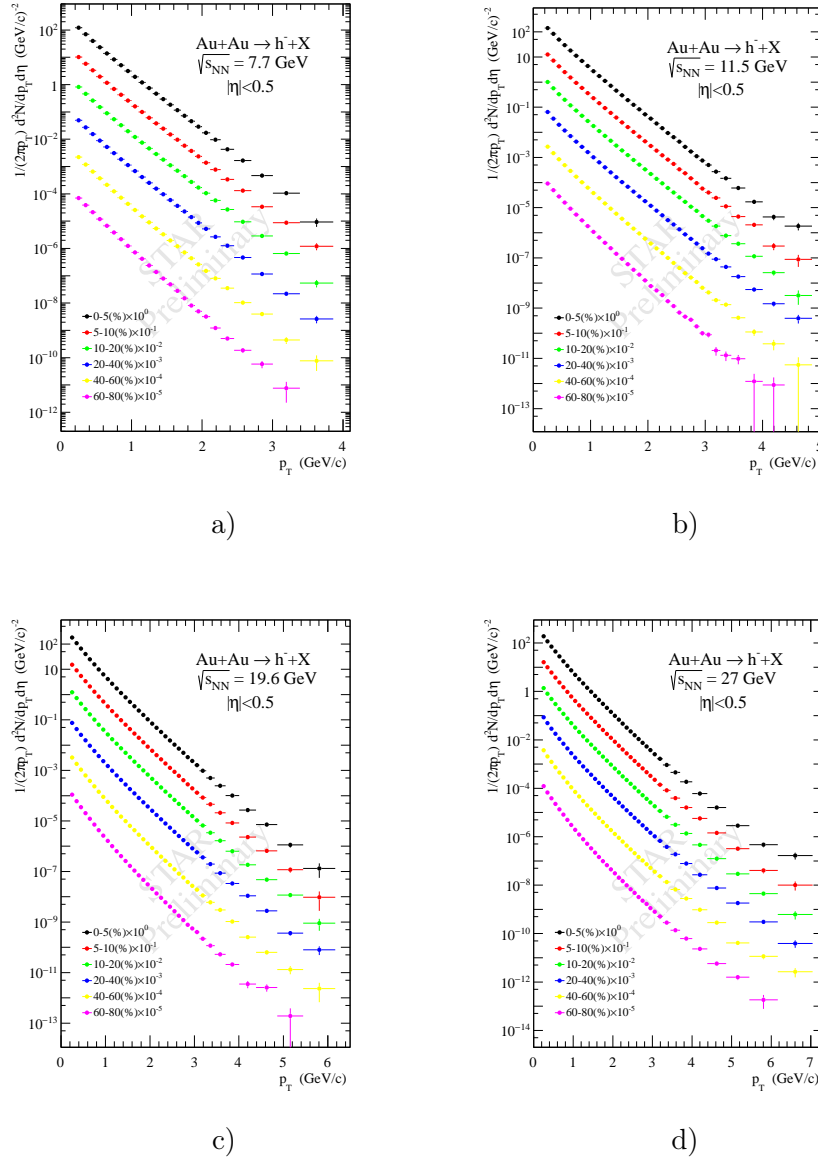


Рис. 3: Transverse momentum spectra of negatively charged particles produced in Au+Au collisions at energies  $\sqrt{s_{NN}} = 7.7, 11.5, 19.6$  and  $27$  GeV in the range  $|\eta| < 0.5$  and for different centralities (0-5%, 5-10%, 10-20%, 20-40%, 40-60%, 60-80%). Errors shown are statistical only.

over a wide momentum range  $0.2 < p_T < 12$ . GeV/c. The multiplied factor of 10 is used for visibility. As seen from Figs. 3 and 4 spectra fall more than eight orders of magnitude. Spectra demonstrate a strong dependence on collision energy and centrality at high  $p_T$ . The exponential behavior of spectra at low  $p_T$  and the power behavior of spectra at high  $p_T$  are observed. Figure 4(d) shows the transverse momentum spectra of negatively charged particles produced in Au+Au collisions at energies  $\sqrt{s_{NN}} = 7.7, 11.5, 19.6, 27, 39, 62.4$  and  $200$  GeV in the range  $|\eta| < 0.5$  for most central events (0 – 5%). The difference in

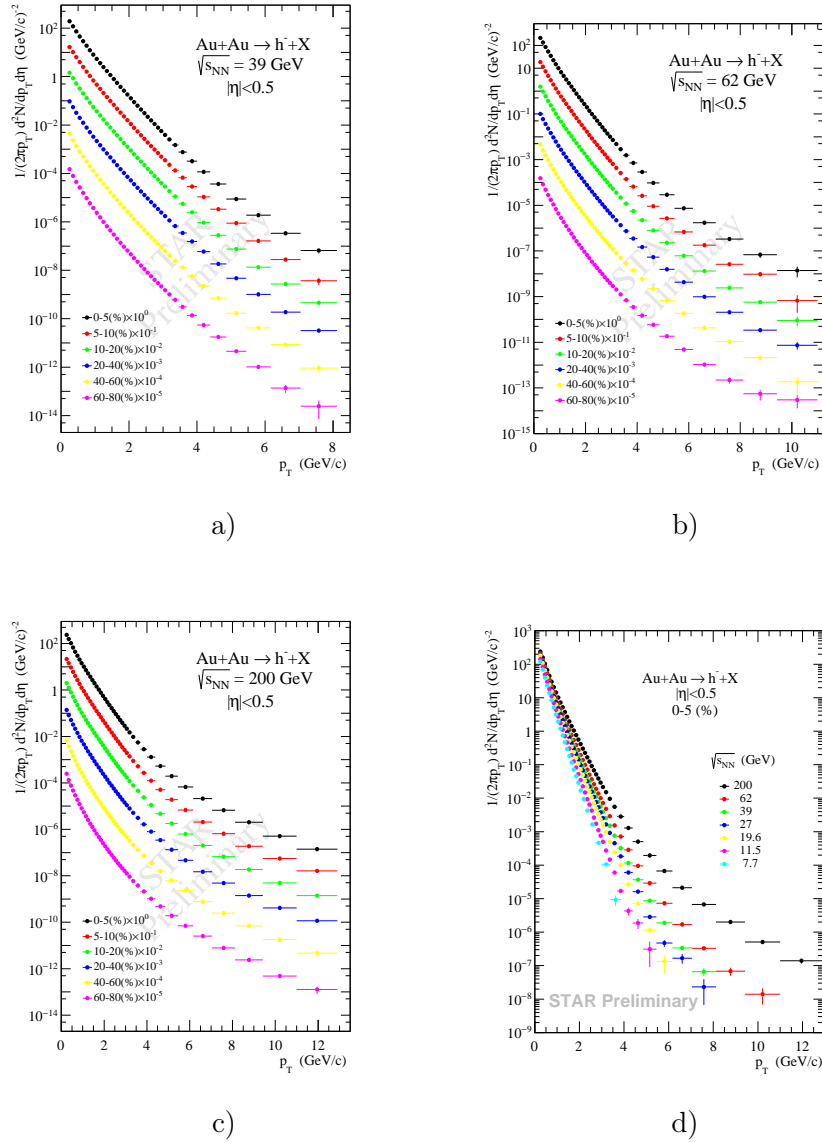


Рис. 4: Transverse momentum spectra of negatively charged particles produced in Au+Au collisions at energies  $\sqrt{s_{NN}} = 39$  (a), 62.4 (b) and 200 GeV (c) in the range  $|\eta| < 0.5$  and for different centralities (0-5%, 5-10%, 10-20%, 20-40%, 40-60%, 60-80%). (d) Spectra for all energies  $\sqrt{s_{NN}} = 7.7 - 200$  GeV in central events (0-5%). Errors shown are statistical only.

particle yields between different energies increases with transverse momentum. It is about three orders of magnitude for 0–5% Au+Au collisions at  $p_T = 5$  GeV/c between energies  $\sqrt{s_{NN}} = 11.5$  and 200 GeV. As we can see the data presentation in terms of dimensional quantities (a particle yield and transverse momentum) demonstrates a strong dependence on the scale.

## B. Self-similarity of negative particle production

The study of critical phenomena in nuclear matter is most preferable in terms of dimensionless variables. The idea of the Beam Energy Scan programs at RHIC is to vary the collision energy and look for the signatures of QCD phase boundary and QCD critical point i.e. to span the phase diagram from the top RHIC energy to the lowest possible energy. Turn-off of signatures of QGP established at  $\sqrt{s_{NN}}=200$  GeV would suggest the crossing of phase boundary.

Self-similarity of hadron interactions is assumed to be a very fruitful concept to study collective phenomena in the hadron and nuclear matter. Important manifestation of this concept is a notion of scaling itself. Scaling in general means self-similarity at different scales. The approach based on  $z$ -scaling suggested in [28–30] is treated as manifestation of the self-similarity property of the structure of colliding objects (hadrons, nuclei), the interaction mechanism of their constituents, and the process of constituent fragmentation into real hadrons. We use the approach for analysis of the obtained spectra (see Figs. 3,4). The approach relies on a hypothesis about self-similarity of hadron interactions at a constituent level. The assumption of self-similarity transforms to the requirement of simultaneous description of transverse momentum spectra corresponding to different collision energies, rapidities, and centralities by the same scaling function  $\psi(z)$  depending on a similarity parameter  $z$ . The scaling function for the collision of nuclei is expressed in terms of the experimentally measured inclusive invariant cross section ( $E d^3\sigma/dp^3$ ), the multiplicity density ( $dN/d\eta$ ), and the total inelastic cross section ( $\sigma_{in}$ ), as follows:

$$\psi(z) = -\frac{\pi}{(dN/d\eta) \sigma_{in}} J^{-1} E \frac{d^3\sigma}{dp^3}. \quad (1)$$

Here  $J$  is the Jacobian for the transformation from  $\{p_T^2, y\}$  to  $\{z, \eta\}$ . The function  $\psi$  is interpreted as a probability density to produce an inclusive particle with the corresponding value of  $z$ . The similarity parameter  $z$  is expressed via momentum fractions ( $x_1, x_2, y_a, y_b$ ), multiplicity density, and parameters  $\delta_{1,2}, \epsilon_{a,b}, c$ , as follows:

$$z = z_0 \Omega^{-1}, \quad (2)$$

where  $z_0 = \sqrt{s_{\perp}} / [(dN_{ch}/d\eta|_0)^c m_N]$ ,  $\Omega = (1 - x_1)^{\delta_1} (1 - x_2)^{\delta_2} (1 - y_a)^{\epsilon_a} (1 - y_b)^{\epsilon_b}$ . Here  $m_N$  is a nucleon mass. The quantity  $\sqrt{s_{\perp}}$  is the transverse kinetic energy of the binary subprocess consumed on the production of the inclusive particle with mass  $m_1$  and its counterpart with mass  $m_2$ . The constituents of the incoming nuclei carry fractions  $x_1, x_2$  of their momenta. The inclusive particle carries the momentum fraction  $y_a$  of the scattered constituent. The parameters  $\delta_{1,2}$  and  $\epsilon_{a,b}$  describe structure of the colliding nuclei and fragmentation process, respectively. The parameter  $c$  is interpreted as a "specific heat" of the created medium. Simultaneous description of different spectra with the same  $\psi(z)$  puts strong constraints on the values of these parameters, and thus allows for their determination. It was found that  $\delta_{1,2}$  and  $c$  are constant at high



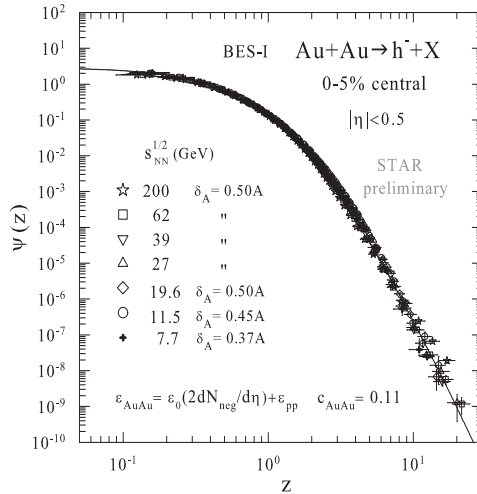


Рис. 5: Scaling function  $\psi(z)$  as a function of self-similarity parameter  $z$  for corresponding transverse momentum spectra of negatively charged particles produced in Au+Au collisions at energies  $\sqrt{s_{NN}} = 7.7 - 200$  GeV in the range  $|\eta| < 0.5$  for most central events (0-5%).

energies,  $\epsilon_{a,b}$  depends on multiplicity and  $m_1 = m_2 \equiv m$ . For the obtained values of  $\delta_{1,2}, \epsilon_{a,b}$  and  $c$ , the momentum fractions are determined to minimize the resolution  $\Omega^{-1}(x_1, x_2, y_a, y_b)$ , which enters in the definition of the variable  $z$ . The system of the equations  $\partial\Omega/\partial x_1 = \partial\Omega/\partial x_2 = \partial\Omega/\partial y_a = \partial\Omega/\partial y_b = 0$  was numerically resolved under the constraint  $(x_1 P_1 + x_2 P_2 - p/y_a)^2 = (x_1 M_1 + x_2 M_2 + m/y_b)^2$ , which has sense of the momentum conservation law of a constituent subprocess [28–30]. The extended version for the approach was applied for description of hadron yields in nucleus-nucleus collisions [30]. The fractal dimension of the nucleus is expressed in terms of the nucleon fractal dimension ( $\delta$ ) and the atomic number of nucleus ( $A$ ) as follows,  $\delta_A = A\delta$ . The fragmentation fractal dimension in nucleus-nucleus collisions is parameterized in the form:  $\epsilon_{AA} = \epsilon_0(dN/d\eta) + \epsilon_{pp}$ . It depends on multiplicity density and nucleon fragmentation dimension ( $\epsilon_{pp} = 0.2$ ). Here  $\epsilon_0$  is a fitting parameter. In this approach the energy loss of the scattered constituent during its fragmentation in the inclusive particle is proportional to the value  $(1 - y_a)$ . We would like to emphasize once more that dimensionless quantities, like momentum fractions, a scaling function and similarity parameter, are expressed via dimensional experimental measurable quantities.

Figure 5 shows scaling function  $\psi(z)$  as a function of self-similarity parameter  $z$ . The data  $z$  presentation corresponds to spectra of negatively charged particles produced in Au+Au collisions at energies  $\sqrt{s_{NN}} = 7.7 - 200$  GeV in the range  $|\eta| < 0.5$  for most central events (0-5%) as a function of the transverse momentum. We observe "collapse" of the data onto a single curve. The solid line is a fitting curve for these data. The derived representation shows the universality of the shape of the scaling curve for the BES energies. The found regularity (the shape of the function and its scaling behavior in the wide kinematic range) can be treated as manifestation of the self-similarity of the

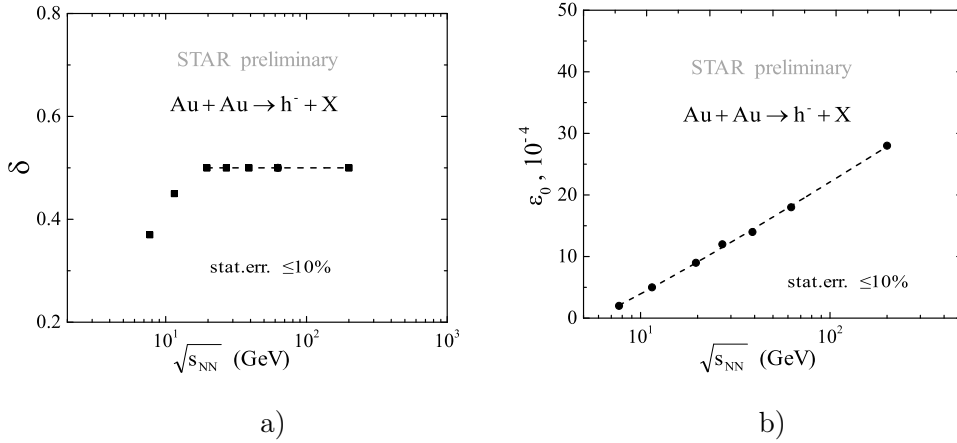


Рис. 6: Model parameters  $\delta$  and  $\epsilon_0$  as a function of collision energy  $\sqrt{s_{NN}}$ .

structure of colliding objects, interaction mechanism of their constituents, and processes of fragmentation of these constituents into real registered particles. As we can see from Fig. 5, the scaling function exhibits two kinds of behavior: one in the low- $z$  and the other in the high- $z$  region. The first regime corresponds to saturation of the scaling function with the typical flattening out. The second one corresponds to the power behavior of the scaling function pointing on self-similarity in constituent interactions at small scales.

### C. Model parameters

The model parameters - nucleus fractal dimension  $\delta_A$ , fragmentation fractal dimension  $\epsilon_{AA}$ , and "heat capacity" $c$ , are determined from the requirement of scaling behavior of  $\psi(z)$  (see Fig. 5) as a function of self-similarity parameter  $z$ . The fractal dimension of the nucleus and the fragmentation dimension are equal to  $\delta_A = A\delta$  and  $\epsilon_{AA} = \epsilon_0(dN/d\eta) + \epsilon_{pp}$ , respectively. Figure 6 shows the dependence of these parameters on the collision energy. It was found that  $\delta$  is independent of the energy for  $\sqrt{s_{NN}} \geq 20$  GeV,  $\epsilon_0$  increases with the energy and  $c$  is independent of the energy over the range  $\sqrt{s_{NN}} = 7.7 - 200$  GeV. Note that, while  $\delta$  decreases with decreased energy for  $\sqrt{s_{NN}} \leq 20$  GeV, the function  $\psi(z)$  preserves the shape in this range.

### D. Constituent energy loss

The nuclear modification factor  $R_{AA}$  measured at RHIC at  $\sqrt{s_{NN}} = 62.4, 130$  and 200 GeV strongly shows a suppression of the charged hadron spectra at  $p_T > 4$  GeV/ $c$ . This suppression [6–9] was one of the first indications of a strong final-state modification of particle production in Au+Au collisions that is now generally ascribed to energy loss of the fragmenting parton in the hot and dense medium. At the BES-I energies the nuclear modification factor drastically changes with a collision energy [14, 20]. It increases with

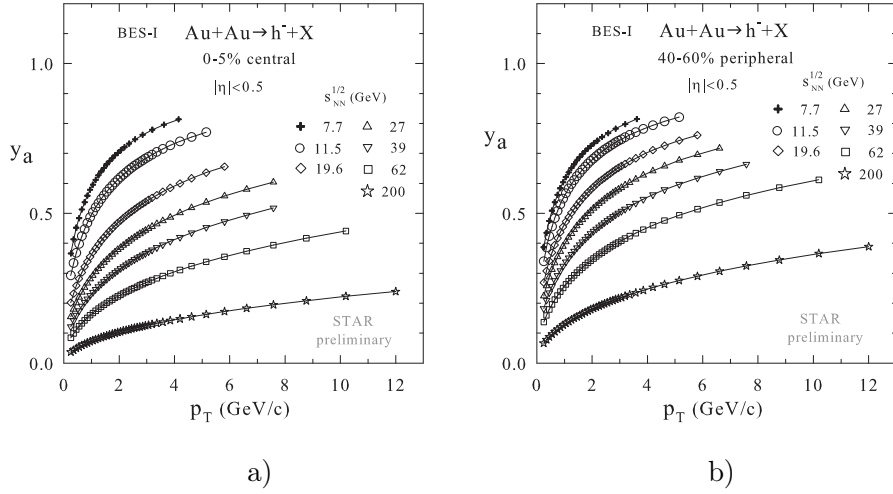


Рис. 7: Momentum fraction  $y_a$  for negatively charged particle production in most central (0–5%) and peripheral (40 – 60%) Au+Au collisions at mid-rapidity ( $|\eta| < 0.5$ ) as a function of the energy  $\sqrt{s_{NN}}$  and hadron transverse momentum  $p_T$ .

transverse momentum as the energy decreases. The study of the evolution of the energy loss with collision energy has relevance to the evolution of created nuclear matter, and can be useful for searching for signature of phase transition and a critical point. The measured spectra (see Fig. 3,4) allow us to estimate constituent energy loss in charged hadron production in Au+Au collisions at BES energies. The estimations are based on a microscopic scenario of particle production proposed in [28–30]. The energy loss of the scattered constituent during its fragmentation in the inclusive particle is proportional to the value  $(1 - y_a)$ .

Figure 7 shows the dependence of the fraction  $y_a$  for central (0 – 5%) and peripheral (40 – 60%) Au+Au collisions on the transverse momentum over a range  $\sqrt{s_{NN}} = 7.7 - 200$  GeV. The behavior of  $y_a$  demonstrates a monotonic growth with  $p_T$ . It means that the energy loss associated with the production of a high- $p_T$  hadron is smaller than that with lower transverse momenta. The decrease of  $y_a$  with collision centrality represents larger energy loss in the central collisions as compared with peripheral interactions. The energy dissipation grows as the collision energy increases. It is estimated to be about 20% at  $\sqrt{s_{NN}} = 7.7$  GeV and 85% at  $\sqrt{s_{NN}} = 200$  GeV for  $p_T \simeq 4$  GeV/c for central events (0 – 5%), respectively. These estimations are in agreement with the energy dependence of the model parameters (see Fig. 6). Discontinuity of these parameters was assumed to be a signature of phase transition and a critical point.

## IV. SUMMARY

In summary, we have presented the first STAR results for negatively charged hadron production in Au+Au collisions at  $\sqrt{s_{NN}} = 7.7 - 200$  GeV from the Beam Energy Scan program at RHIC. The spectra of particle yields at mid-rapidity were measured over a wide range of transverse momentum. The spectra demonstrate a strong dependence on the collision energy and centrality which enhances with  $p_T$ . An indication of self-similarity of negatively charged particle production in Au+Au collisions was found. It is seen in the presentation of spectra by scaling function  $\psi$  in dependence on self-similarity parameter  $z$  for all energies.

The obtained spectra of negatively charged hadrons in Au+Au collisions were used to estimate of a constituent energy loss as a function of energy and centrality of collisions and transverse momentum of inclusive particle in the  $z$ -scaling approach. It was shown that the energy loss increases with the collision energy and centrality, and decreases with  $p_T$ .

The energy dependence of the model parameters - the fractal and fragmentation dimensions and "specific heat was studied. All parameters demonstrate smooth behavior with energy for most central events. It is expected that the second phase of BES will allow us to clarify the existence of a discontinuity and strong correlation of these parameters with much higher statistics.

The presented results provide an additional motivation for the Beam Energy Scan-II at the STAR experiment [14, 20]. The large and uniform acceptance and extended particle identification is suitable for a critical point search. The BES Phase-II program will allow for high-statistics measurements, with an extended kinematic range in rapidity and transverse momentum, using sensitive observables, to reveal the structure of the QCD phase diagram [20].

- 
- [1] K. Fukushima and T. Hatsuda, *Rept. Prog. Phys.* **74**, 014001 (2011).
  - [2] BRAHMS Collab. (I. Arsene *et al.*), *Nucl. Phys. A* **757**, 1 (2005).
  - [3] PHOBOS Collab. (B.B. Back *et al.*), *Nucl. Phys. A* **757**, 28 (2005).
  - [4] STAR Collab. (J. Adams *et al.*), *Nucl. Phys. A* **757**, 102 (2005).
  - [5] PHENIX Collab. (K. Adcox *et al.*), *Nucl. Phys. A* **757**, 184 (2005).
  - [6] STAR Collab. (J. Adams *et al.*), *Phys. Lett. B* **616**, 8 (2005).
  - [7] STAR Collab. (J. Adams *et al.*), *Phys. Lett. B* **637**, 161 (2006).
  - [8] STAR Collab. (B.I. Abelev *et al.*), *Phys. Rev. Lett.* **97**, 152301 (2006).
  - [9] STAR Collab. (B.I. Abelev *et al.*), *Phys. Lett. B* **655**, 104 (2007).

- [10] STAR Collab. (B.I. Abelev *et al.*), *Phys. Rev. C* **77**, 54901 (2008).
- [11] STAR Collab. (J. Putschke *et al.*), *J. Phys. G: Nucl. Part. Phys.* **34**, 5679 (2007).
- [12] STAR Collab. (M. Daugherty *et al.*), *J. Phys. G: Nucl. Part. Phys.* **35**, 104090 (2008).
- [13] STAR Collab. (B.I. Abelev *et al.*), *Phys. Rev. C* **80**, 064912 (2009).
- [14] STAR Collab. (B. Abelev *et al.*), *Phys. Rev. C* **81**, 024911 (2010).
- [15] B. Mohanty, *Nucl. Phys. A* **830**, 899c (2009).
- [16] STAR Collab. (L. Kumar), *Nucl. Phys. A* **830**, 275c (2009).
- [17] STAR Collab. ( M. Aggarwal *et al.*), arXiv:1007.2613v1 [nucl-ex] 15 Jul 2010(2010).
- [18] STAR Collab. (L. Kumar), *Nucl. Phys. A* **904-905**, 256c (2013).
- [19] L. Kumar, *Mod. Phys. Lett. A* **28**, 1330033 (2013)
- [20] STAR Collab. *STAR Note* **SN0598**, 1 (2014).
- [21] H.E. Stanley, Introduction to Phase Transitions and Critical Phenomena (Oxford, New York and Oxford) 1971.
- [22] H.E. Stanley, *Rev. Mod. Phys.* **71**, S358 (1999).
- [23] STAR Collab. ( K.H. Ackermann *et al.*), *Nucl. Instr. Meth. A* **499**, 624 (2003).
- [24] T. Zou *et al.* *Nucl. Instrum. Meth. A* **605**, 282 (2009).
- [25] STAR Collab. (W.J. Llope *et al.*), *Nucl. Instr. Meth. A* **522**, 252 (2004).
- [26] STAR Collab. (B. Abelev *et al.*), *Phys. Rev. C* **79**, 034909 (2009).
- [27] STAR Collab. (B. Abelev *et al.*), *Phys. Rev. C* **81**, 024911 (2010).
- [28] I. Zborovský and M.V. Tokarev, *Phys. Rev. D* **75**, 094008 (2007).
- [29] I. Zborovský and M.V. Tokarev, *Int. J. Mod. Phys. A* **24**, 1417 (2009).
- [30] M.V. Tokarev and I. Zborovský, *Phys. Part. Nucl. Lett.* **7**, 171 (2010).